Nature Communications

https://doi.org/10.1038/s41467-026-70569-y

Article in Press

Self-reorganization and information transfer in large-scale models of fish schools

Received: 8 April 2025

Accepted: 25 February 2026

Cite this article as: Hang, H., Huang, C., Barnett, A. *et al.* Self-reorganization and information transfer in large-scale models of fish schools. *Nat Commun* (2026). https://doi.org/10.1038/s41467-026-70569-y

Haotian Hang, Chenchen Huang, Alex Barnett & Eva Kanso

Self-reorganization and Information Transfer in Large-scale Models of Fish Schools

Haotian Hang[1], Chenchen Huang[1], Alex Barnett[2], Eva Kanso[1,3*]

[1]Department of Aerospace and Mechanical Engineering, University of Southern California, Los Angeles, CA 90089
[2]Center for Computational Mathematics, Flatiron Institute, New York City, NY 10010
[3]Department of Physics and Astronomy, University of Southern California, Los Angeles, CA 90089

February 24, 2026

Abstract

The remarkable cohesion and coordination of moving animal groups and their collective responsiveness to threats are often attributed to scale-free correlations, where behavioral changes in one animal influence others in the group, regardless of the distance between them. But are these features independent of group size? Here, we investigate group cohesiveness and collective responsiveness in computational models of massive schools of fish of up to 50,000 individuals. We show that as the number of swimmers increases, flow interactions destabilize the school, creating clusters that constantly fragment, disperse, and regroup, much like in natural animal groups. Importantly, while spatial correlations in cohesive and polarized clusters are indeed scale free, fragmentation events are preceded by a decrease in correlation length, weakening the group's collective responsiveness and leaving it more vulnerable to predation. We further show that information about directional changes propagates linearly in time among group members, thanks to the non-reciprocal nature of visual interactions between individuals. Merging events speed up this information transfer, while fragmentation slows it down. Our findings suggest that flow interactions may have played an important role in group size regulation, behavioral adaptations, and dispersion in living animal groups.

Introduction

Nature is in a perpetual state of reorganization. In animal groups on the move, such as in bird flocks [1–3], fish schools [4–6], and insect swarms [7–9], local social interactions result in cohesive global patterns [4, 10–14]. However, while these cohesive patterns are regularly documented in systems of small or moderate size [4, 6, 15–19], it is unclear how they scale with increasing group size [20]: do large groups remain cohesive or do they undergo dynamic reorganization? We

*Corresponding author: Kanso@usc.edu

address this question in massive simulations of schooling fish, where individual swimmers interact through self-generated flows and follow behavioral rules inferred directly from experimental data in shallow water environments [6, 16, 17, 21]. By optimizing our computational algorithms, we simulate over long times the motion of groups of up to 50,000 fish. We show that "more is different" [22, 23]. Where smaller groups maintain cohesive and polarized formations, larger groups spontaneously reorganize, constantly fragmenting, scattering and reassembling, similarly to empirical observations of large flocks of birds [1, 2] and schools of fish [20, 24–26]. We analyze how this self-reorganization influences the collective responsiveness and speed of information propagation between members of the group [1, 4, 27].

Collective responsiveness in self-organized animal groups manifests in long-ranged spatial correlations [1, 28, 29]. Correlation measures how the change in the behavior of one individual influences the behavior of others in the group. An animal group exhibits maximal responsiveness to a perturbation, say, caused by an attacking predator [20, 30], when correlations are scale-free, that is, when the range of spatial correlations scales with the linear group size [1, 30]. Analysis of empirical data of large bird flocks confirms that spatial correlations scale linearly with group size L [1]. But do these results translate to groups of swimmers?

In physical models of flow-coupled swimmers, microscopic [31–33] and inertial [18, 34–36], fluctuations get amplified as they propagate via the fluid medium, hindering group cohesion. These models do not enable individual swimmers to sense and actively respond to flows. Biological swimmers, on the other hand, are flow sensitive [37–39] and seem to correlate their tailbeat frequencies and phase [40–42], but the extent of flow-mediated correlations is limited in space [18]. Recent evidence suggests that vision is both necessary and sufficient for polarized schooling [43]. Even in robotic agents, active response to visual cues is sufficient to produce scale-free correlations in polarized collectives [44]. But are these scale-free correlations universal to groups of individuals with long-ranged visual and hydrodynamic interactions? If so, how does dynamic reorganization within the group, including splitting and merging event, affect the extent of spatial correlations? Statistical analysis in the context of our schooling model reveals

that spatial correlations in cohesive and polarized groups are indeed scale free, much like in natural animal groups, but the correlation length decreases prior to fragmentation. This loss of scale-free correlations serves as a predictive marker of fragmentation.

Spatial correlations reflect the extent of information spread within a group but fail to capture the dynamic nature of information propagation. How fast does information travel within a polarized group? Motivated by analyses of information propagation in bird flocks [27], we approach this question by considering the behavior of our interacting swimmers during spontaneous collective turns. We find that the information about the change in direction propagates linearly in time across the group, at speeds much faster than the individual swimming speed. This is in sharp contrast to the diffusive information propagation in symmetric consensus-based models [10], and in the absence of behavioral inertia [27]. We show that symmetry is broken due to the non-reciprocal nature of the interactions between individual swimmers [45, 46]. We further find that merging of separate clusters speeds up the transfer of information within each cluster by several folds, while fragmentation slows it down. Interestingly, flow interactions enhance the information travel speed beyond what would be expected from non-reciprocal visual interactions alone.

Results

Mathematical Model. Consider a system of N fish, where each fish is represented as a self-propelled particle moving at a constant speed U ($\mathrm{m{\cdot}s^{-1}}$) relative to the flow velocity. Each fish follows behavioral rules, derived empirically from shallow-water experiments [6, 15], modulated by an asymmetrical visual field representing frontal-biased perception [6]. Additionally, each fish creates a flow disturbance represented by its far-field potential dipole (Fig. 1A) [34, 47] and responds to the combined flow generated by all other swimmers [16, 17].

Let fish i be located at $\mathbf{x}_i \equiv (x_i, y_i)$ in an inertial (x, y)-frame and have a heading direction $\mathbf{p}_i \equiv (\cos\theta_i, \sin\theta_i)$ expressed in terms of the orientation angle θ_i measured from the x-axis. The velocity $\mathbf{v}_i = \dot{\mathbf{x}}_i$, where $\dot{()}$ represents derivative with respect to time t, and the change of heading

angle $d\theta_i$ are governed by the equations of motion, written directly in non-dimensional form, with swimming speed $U = 1$,

$$\begin{aligned} \dot{\mathbf{x}}_i &= \mathbf{v}_i = U\mathbf{p}_i + \mathbf{U}_i, \\ d\theta_i &= \frac{\sum_{j\in\mathcal{V}_i}\left(r_{ij}\sin\theta_{ij} + I_a\sin\phi_{ij}\right)\left(1+\cos\theta_{ij}\right)}{\sum_{j\in\mathcal{V}_i}\left(1+\cos\theta_{ij}\right)}dt + \Omega_i dt + I_n dW_t. \end{aligned} \tag{1}$$

The first term on the right-hand side of the orientation equation represents the fish change in heading in response to visual feedback: fish i only "sees" its Voronoi neighbors $\mathcal{V}_i$, with attraction intensity normalized to one and non-dimensional alignment intensity I_a, both averaged with weight $1 + \cos\theta_{ij}$ modeling continuously a rear blind angle [15] (Fig. 1B). The intermediate variables $r_{ij} = \|\mathbf{x}_i - \mathbf{x}_j\|$, $\theta_{ij} = (\angle(\mathbf{x}_j - \mathbf{x}_i) - \theta_i)$, and $\phi_{ij} = \theta_j - \theta_i$ represent, respectively, the relative distance, viewing angle, and difference in heading angle between fish i and j. The non-dimensional noise intensity I_n scales a standard Wiener process $W(t)$ modeling the fish "free will" [48].

The vector $\mathbf{U}_i$ represents the flow velocity generated by all other swimmers at the location of swimmer i and Ω_i denotes the angular velocity

$$\mathbf{U}_i = \sum_{j=1, j\neq i}^{N} \frac{I_f}{\pi}\frac{\mathbf{p}_j^{\perp}\sin 2\theta_{ji} + \mathbf{p}_j\cos 2\theta_{ji}}{r_{ij}^2}, \qquad \Omega_i = \mathbf{p}_i \cdot \frac{d\mathbf{U}_i}{d\mathbf{x}}|_{\mathbf{x}_i} \cdot \mathbf{p}_i^{\perp}, \tag{2}$$

where $\mathbf{p}^{\perp}$ is a unit vector orthogonal to $\mathbf{p}$ and I_f is the strength of fish-induced dipolar flow field, which, by definition, introduces a dimensionless length scale $a = \sqrt{I_f/U}$ reflecting the swimmer's bodylength [47]. Eqs. (1)– (2) form a closed set of $3N$ differential equations governing the $3N$ unknowns (x_i, y_i, θ_i), where $i = 1, \ldots, N$. These equations depend solely on three non-dimensional parameters, I_n, I_a, and I_f, representing the noise, alignment, and hydrodynamic intensities.

Fixing the hydrodynamic intensity and varying the noise and alignment intensities in groups of $N = 100$ fish produces distinct collective phases, from swarming to polarized schooling [16]. In polarized schools, the dipolar hydrodynamic interactions represented by $\mathbf{U}_j$ destabilize side-

by-side configurations, favoring in-line arrangements (Fig. S1) [31, 34, 47]. This hydrodynamic drafting increases the school's average velocity, given by $\langle \mathbf{v} \rangle = \frac{1}{N} \sum_{j=1}^{N} \dot{\mathbf{x}}_j = \frac{1}{N} \sum_{j=1}^{N} (U\mathbf{p}_j + \mathbf{U}_j)$, causing the group to swim, on average, faster than the individual swimming speed U [16].

Dynamic reorganization, fragmentation, dispersal, and reassembly in large fish schools. Using (1)-(2), we numerically simulated the motion of a school of 50,000 fish coupled via visual feedback rules and flow interactions in an unbounded planar domain (Fig. 1, Suppl. Movie 1). Here, we used parameter values (I_n, I_a, I_f) that, in smaller groups of 100 fish, led to stable polarized schooling [16, 17] (Fig. 2A). We optimized our computational algorithms in order to scale our simulations to groups of the order of 10^4 swimmers (Methods). In the group of 50,000 fish, starting from random initial conditions, the fish self-organized into coherent polarized structures that dynamically fragmented and reassembled, exhibiting large density fluctuations (Fig. 1, Suppl. Movie 1), comparable to empirical observations of large bird flocks [1] and fish schools [20, 24–26].

We systematically varied the number of swimmers N. In Fig. 2A-C, we report cohesive and highly polarized schools of 100 and 1000 swimmers and loss of global cohesion in a school of 10,000 swimmers, where distinct polarized clusters moved in different directions. Statistical results from sample simulations at $N = 100$, 1000, 10,000, and 50,000 are reported in Fig. 2D-G. The polarization order parameter $P = \| \sum_{j=1}^{N} \mathbf{p}_j \| / N$ is consistently close to 1 for $N = 100$ and 1000, indicating high polarization at all time. For N= 10,000 and 50,000, P fluctuates violently, reflecting the reorganization and constant splitting and merging in larger schools: a sharp decrease in P indicates a splitting event, while a sharp increase indicates a merging event.

Considering the average velocity $\langle \mathbf{v} \rangle = \sum_{j=1}^{N} \mathbf{v}_j / N$ of the entire school, we found that, on average, schools swam faster than the individual self-propelled speed U for N =100 and 1000 because of flow interaction, consistent with [16], but slower for N =10,000 and 50,000 because these larger schools broke up into subgroups that themselves swam faster but in random directions. This increase in the speed of the polarized clusters is due to hydrodynamic interactions (1-2). For example, in the snapshots in Fig. 2A-C, the school moved at an average speed of 1.20 at

$N = 100$, 1.08 at $N = 1000$, and 0.54 at N =10,000. The highly-polarized clusters that formed within the larger schools could reach equally high speeds as their free counterparts; in Fig. 2C, the four clusters moved at speeds 1.14, 0.83, 0.86, 1.08, but in different directions leading to an overall speed of 0.54 (Suppl. Movie 2). The time evolution of $\cos(\angle\langle\mathbf{v}\rangle)$, where $\angle\langle\mathbf{v}\rangle$ represents the school's overall orientation, shows more frequent changes in orientation at smaller N, whereas in the larger schools, frequent splitting and merging events create subgroups that move in random directions, hindering the entire school from turning together cohesively. Fig. 2F and G show the number of subgroups per school identified by a density-based clustering algorithm (Methods, [49–51]) and the average number of fish per cluster. The larger schools at N= 10,000 and 50,000 exhibited wider distributions, reminiscent of empirical observations [25], suggesting the existence of a capacity of number of swimmers per polarized cluster that follows a distribution skewed towards moderate values, with a heavy tail beyond which the cluster breaks up and reorganizes. Because of the behavioral and statistical similarities between N= 10,000 and N = 50,000, and to save computational effort, hereafter we investigate the mechanisms responsible for this behavior in groups of up to 10,000 fish.

Transition from cohesion to fragmentation in larger schools. In Fig. 3A, we report the time-averaged values of the school polarization P as a function of N. As we varied N from 100 to 10,000, up to $N \approx 1000$, the swimmers exhibited stable schooling, behaving mostly as an indivisible entity, with consistently high polarization values P greater than 0.95. Beyond $N = 1000$, the school began to fragment, forming locally polarized subgroups that dynamically rejoined and separated again. This indicates the existence of a bifurcation depending on school size, past which the dynamic reorganization within the school caused a decrease in the global polarization order parameter and an increase in its variance (Fig. 3A). In the highly polarized and cohesive regime, the school turned frequently and rarely fragmented, but as N increased, the frequency of global turning events decreased while the frequency of splitting and merging increased (Fig. 3B).

Flow interactions trigger spontaneous reorganization within the school. We next asked what mechanisms lead to the school fragmentation and self-reorganization at larger N. Given that our model accounts for vision-based rules of alignment and attraction, flow interactions, and individual noise, we set out to test the role of each in triggering the transition from the cohesive state to the state of self-reorganization with increasing school size. We first suppressed all hydrodynamic interactions, and considered a school of 10,000 swimmers interacting only via vision-based rules. We observed no fragmentation, reassembly, and reorganization, independent of noise levels (Supplementary Fig. S2D). At exceedingly large noise, the school transitioned to a swarming phase where all polarization was lost, consistent with classic models [4, 5, 13, 15, 16]. We thus concluded that the vision-based rules of attraction and aligning to Voronoi neighbors lead to no fragmentation of the group, independent of group size, and that noise alone is not sufficient for self-reorganization. Hydrodynamic interactions are important. With hydrodynamic interactions and no noise, the phenomena of dynamic reorganization, fragmentation, dispersal, and reassembly remain largely unchanged (Fig. S3). At a fixed dipole intensity, varying the noise intensity has little effect on the collective pattern (Fig. 3C). These results imply that the transition from cohesive schooling to self-reorganization is driven by flow interactions. To explore the threshold of this flow-induced instability, we maintained the same noise level and varied the intensity of the hydrodynamic interactions by increasing the dipolar field I_f across several orders of magnitudes from 10^{-4} to 5: since $I_f \sim a^2 U$ is proportional to the swimmer's speed U and the square of the bodylength a, a weaker dipolar intensity represents smaller and slower fish and a larger dipolar intensity represents larger and faster fish [16]. In Fig. 3D, we report results across this wide range of I_f for $N = 100$, 1000, and 10,000 swimmers. Smaller schools maintain school cohesion at larger values of I_f. In larger schools, cohesion is lost at smaller values of I_f, indicating that the capacity for cohesive schools depends on the hydrodynamic intensity of individual swimmers, which in turn depends on their size and speed. That is, smaller fish can school cohesively in larger numbers (Fig. 3E).

Scale-free correlation breaks down during school self-reorganization. The range of spatial correlations in polarized flocks of birds was shown to scale with the maximal length of the flock [1]. This linear scaling of correlation length with group size implies that the effective perception range of each individual encompasses the entire group and enables transfer of information between members regardless of distance, ensuring collective response to perturbations [1, 2, 26]. We asked whether these conclusions are generic to emergent polarization in groups of self-propelled individuals, including our simulations of schooling fish, and how self-reorganization within the school, in the form of continuous fragmentation, dispersal, and reassembly, affects the range of spatial correlation and the ability to transfer information among school members.

To address these questions, we first considered cohesive and highly polarized groups of swimmers ranging in size from $N = 100$ to 1000, where consistent with [1], we analyzed snapshots with high degree of polarization ($P > 0.9$). For swimmer i, we defined the fluctuation $\delta\mathbf{v}_i$ around the group's mean velocity as $\delta\mathbf{v}_i = \mathbf{v}_i - \langle\mathbf{v}\rangle$ (Fig. 4A,B). By construction, $\sum_{i=1}^{N} \delta\mathbf{v}_i = \mathbf{0}$, indicating no net fluctuations in the net motion of the center of mass of the school. We calculated the spatial correlation function $C(r)$ of velocity fluctuations (Methods), where the span of r does not exceed the length L of the group defined as $L = \max \|\mathbf{x}_i - \mathbf{x}_j\|$. A positive value of $C(r)$ close to 1 implies that the fluctuations are nearly parallel and strongly correlated. Conversely, a negative value of $C(r)$ close to -1 implies that the fluctuations are antiparallel and anticorrelated. A value of $C(r) \approx 0$ implies a random distribution of velocity fluctuations with no correlation. In Fig. 4C, we report $C(r)$ versus r for the snapshot presented in Fig. 4A. At short distances, the correlation is close to 1 and decays with increasing r, becoming negative at large interindividual distances, indicating strong correlation at short distances and strong anticorrelation at large distances, and in no range of r are the velocity fluctuations uncorrelated.

To explain the behavioral implications of this form of $C(r)$, we defined the correlation length ξ as the relative distance r at which $C(\xi) = 0$. By definition, the value of ξ is the maximal size of the positively correlated domain. In Fig. 4D, the resulting correlation length ξ is plotted versus school length L using simulations at various sets of parameters (I_f, I_a, I_n) and school size

$N \leq 1000$, provided $P > 0.9$ (Table S1). We found that ξ increases linearly with L, much like in the case of starling flocks [1]. We found no scale-free behavior in speed correlations, because speed fluctuations in our model are due to passive hydrodynamic interactions and do not arise from active interactions between the swimmers (Fig. S4). These results confirm that scale-free correlations in velocity fluctuations are generic. They reflect the rotational interactions encoded at the level of individual swimmers (Eq. 1), and can be attributed to the existence of a Goldstone mode associated with the breaking of rotational symmetry leading to group polarization [52, 53]. Interestingly, in our simulations, the slope of the best fit of ξ vs L is nearly one-third, similar to the slope reported in [1] for natural bird flocks.

But does this scale-free correlation generalize to larger groups that continuously reorganize? To answer this question, we revisited the simulation of $N = 10{,}000$ fish reported in Fig. 2 and identified cohesive and highly polarized clusters within the school that are about to undergo self-reorganization. In Fig. 4E, we report a snapshot where the entire school moves cohesively, at high polarization, preceding a splitting event, where the school fragments into three different clusters (highlighted in different colors). We calculated the time evolution of the polarization parameter P of the entire school and of the subgroups that later constituted the three separate clusters (Fig. 4F). The school maintained a high level of polarization until the time at which it fragmented, beyond which P decreased, but each cluster recovered quickly, exhibiting high polarization per cluster. Interestingly, a gradual decrease in the correlation length ξ far preceded the sharp decrease in P, while the school size L remained unchanged (Fig. S5E), inducing an overall decrease in ξ/L over time and loss of scale-free correlation prior to fragmentation. This loss in scale-free correlation is predictive of an upcoming splitting event in all cohesive clusters.

To verify this, we considered the time evolution of the school of 10,000 swimmers and, at each snapshot, we identified all clusters of cohesive swimmers, selected highly-polarized clusters for which $P > 0.9$, calculated the corresponding ξ and L, and plotted the joint probability density function of cluster size L and correlation length ξ as a heatmap over the (L, ξ) space (Fig. 4G). The (L, ξ) values are concentrated at and below the scale-free correlation line (dashed grey)

obtained in stable schools in Fig. 4D. Highlighted on this plot are the (L, ξ) values corresponding to the fragmentation event reported in Fig. 4E,F: the correlation length starts at the scale-free line $\xi/L \sim 1/3$ and decreases before the onset of splitting (grey arrow), emphasizing the loss of scale-free correlation during school reorganization.

Loss of scale-free correlation is a predictive marker of fragmentation. To support our finding that loss of scale-free correlation is a precursor to fragmentation, we revisited the case of $N = 1000$. At $N = 1000$, fragmentation events are isolated and thus simpler to analyze, as opposed to the school of 10,000 fish where multiple fragmentation events could occur simultaneously. We conducted 10 Monte Carlo simulations at $N = 1000$ for a total duration of 1000 time units each.

In Fig. 5A, we show snapshots of a splitting and merging event, and in Fig. 5B, we show the time evolution of the polar order parameter P, school size L, correlation length ξ and ratio of correlation length to school size ξ/L over a time window before and including a single fragmentation and merging event (highlighted in grey). Before the onset of fragmentation, the polarization P and school size L remain relatively stable. After fragmentation, the school size L increases and then decreases during merging. Importantly, ξ and ξ/L seem to decrease prior to the onset of fragmentation. To quantify this decrease in correlation length prior to fragmentation, we analyzed the time evolution of all 10 Monte Carlo simulations, discarding the initial 200 time units to ensure that the school has reached steady state. We then identified the time t^* marking the onset of each fragmentation event and the time $t^\dagger$ marking the end of merging following fragmentation, and took the time average of P, L, ξ, and ξ/L over a time window starting at the end of the preceding merging event and ending 100 time units prior to the onset of the next fragmentation event. We also averaged these values over a time window starting at $t^* - \tau$ and ending at the onset of fragmentation t^*. We tested four different values of $\tau = 10$, 30, 50 and 100. Collecting the statistics from all simulations (Fig. 5C), we found that the polar order parameter P and school size L were largely insensitive to the temporal placement of the averaging window, far or right before a fragmentation event. However, the correlation

length ξ and ratio ξ/L decreased significantly right before a fragmentation event. These results reinforce our conclusion that the correlation length decreases prior to fragmentation and that this decrease serves as a predictive marker of fragmentation.

Information propagates linearly in time in cohesive groups. Spatial correlations reflect the extent of information spread within a group but do not describe the dynamics of information propagation nor the efficiency of a collective response to environmental factors [1, 27, 52]. An efficient collective response depends on how fast localized perturbations succeed in modifying the behavior of the entire group. Take, for example, a group changing its overall heading direction (Fig. 6A and Suppl. Movie 3). The actual execution of such turn is not instantaneous, because a certain amount of time is needed to propagate the turn throughout the group. During this time, cohesion is strained by the mismatch between individuals who have already turned and those who have not yet done so, as reflected by a drop in polarization P (Fig. S5B). Therefore, the speed at which information is transferred from individual to individual plays a crucial role in maintaining group cohesion, which in return is key for scale-free correlation and collective responsiveness.

We set out to quantify information transfer in cohesive groups first, then to assess the effect of school reorganization – fragmentation and merging – on information transfer. To fix ideas, we analyzed, following [27], a collective turn in a cohesive group of $N = 1000$ swimmers. Given the trajectory of each swimmer i (Fig. 6A), we calculated the curvature κ_i as a function of time and identified the time t_i of maximum curvature. For each pair of swimmers, i and j, we calculated their mutual turning delay, $\tau_{ij} = t_i - t_j$, defined as the amount of time by which swimmer j turns before ($\tau_{ij} > 0$) or after ($\tau_{ij} < 0$) swimmer i (Methods, Fig. 6B, inset, and S5C). From the delays τ_{ij}, we ranked all swimmers in the group according to their turning order and labeled each swimmer i by its order o_i in terms of its absolute turning time t_i with respect to the top-ranking swimmer. We found that the top-ranking swimmers – the first swimmers to turn – are physically close to each other (Fig. 6C, inset). That is, the collective turn has a spatially localized origin and propagates anisotropically from front to back through swimmer-to-swimmer transmission

of information.

Given that the motion of the group is two-dimensional and that the turn has a localized origin, the information propagates a distance $d_i = \sqrt{o_i/\rho}$, where ρ is the school density, which remains nearly constant during the turn. Plotting d_i versus time (Fig. 6C), we found a clear linear regime at early and intermediate times, implying that the distance traveled by the information grows linearly with time $d(t) = ct$, where c is the speed of propagation of information; its value is about 20 times that of the self-propelled speed U of individual swimmers in our model. We repeated this analysis for various turning instances in schools ranging in size from 100 to 2000 swimmers (Fig. S6). The information transfer speed fluctuated with the number of swimmers but remained consistently an order of magnitude larger than that of the individual swimming speed (Fig.7B).

Information travels linearly thanks to non-reciprocal visual interactions. The linear and fast propagation of information within the school is a key factor in preserving school cohesion during turning. What is the mechanism responsible for this phenomenon? Theoretical models based on local alignment with neighboring individuals, such as the Vicsek model [10], lead to diffusive information propagation, with speeds that scale sublinearly with $\sqrt{t}$ [27]. In [27], to account for the linear propagation speed of directional changes observed in empirical data of bird flocks, the authors introduced behavioral inertia into the alignment dynamics. This modification transformed the diffusive model into a wave equation, allowing information to propagate both forward and backward across the group. However, our results are based on a kinematic model (1)- (2) that ignores the inertia of the fluid and individual swimmers. In our model, the key ingredient enabling information to propagate linearly in time is the non-reciprocal nature of visual interactions between individuals.

To explain the role of non-reciprocal vision in information propagation within the group, we set out to derive a continuum partial differential equation governing the phase φ, where $\varphi_i = \theta_i - \langle\theta\rangle$ is the perturbation from the school average heading direction $\langle\theta\rangle = \angle\mathbf{v}$. Ignoring

noise and flow interactions, and starting from the alignment dynamics in (1), we get

$$\dot{\theta}_i = I_a \frac{\sum_{j\in\mathcal{V}_i} \sin\phi_{ij}(1+\cos\theta_{ij})}{\sum_{j\in\mathcal{V}_i}(1+\cos\theta_{ij})}. \tag{3}$$

Considering, with no loss of generality, $\langle\theta\rangle = 0$ and assuming the swimmers are located on a two-dimensional square lattice of mesh size α, we coarse-grain (3) over a box containing a focal swimmer and four immediate neighbors and take the continuous limit to arrive at

$$\frac{\partial\varphi}{\partial t} = \frac{\alpha^2 I_a}{4}\Delta\varphi + \frac{\alpha I_a}{2}\left(\frac{\partial\varphi}{\partial x} + \varphi\frac{\partial\varphi}{\partial y}\right) \approx \frac{\alpha^2 I_a}{4}\Delta\varphi + \frac{\alpha I_a}{2}\frac{\partial\varphi}{\partial x}. \tag{4}$$

The equation governing φ has an anisotropic advection term, where φ is advected linearly in the longitudinal direction and non-linearly in the transverse direction, albeit at much smaller and thus ignorable speed (considering that $\varphi \ll 1$). The diffusion term scales with $\alpha^2 I_a$, while the advection term scales with αI_a, implying that in dense schools, linear advection is dominant. That is, unlike the second-order wave equation in [27], information here is governed by a first-order transport equation. Ignoring diffusion and considering an initial perturbation $\varphi_0(x,y) = A\sin(kx)$ in the longitudinal x-direction of amplitude A and wavelength k, the perturbation propagates from front to back at a speed $c = \alpha I_a/2$, following $\varphi(t,x,y) = A\sin(k(x+ct))$.

To test the prediction that information propagates linearly from the front to the back of the school at speed $c \propto \alpha I_a$ in numerical simulations with noise and flow interactions, we systematically varied both the alignment and noise intensities and calculated the resulting polarization P in cohesive groups (Figs. 7A, S9). We found that P satisfies the relation $P = 1 - I_n/I_a$ derived in [27] using the spin-wave approximation. We also calculated the information transfer speed c during turning as a function of I_a/I_n and found that, indeed, c scales linearly with I_a/I_n (Fig. 7C), demonstrating consistency between our simulations and the scaling law derived from the alignment model. Our results uncover a vision-based mechanism for linear information propagation, distinct from the behavioral inertia proposed in [27]. Indeed, our results differ from [27] in two ways: c scales linearly with alignment intensity I_a, in contrast to the sublinear

scaling $c \propto \sqrt{I_a}$ in [27], and information propagates from the front to the back of the school, as opposed to the isotropic information propagation in [27]. Importantly, our theory shows an anisotropy in the information transfer speed, with information traveling faster in the longitudinal direction of the school. Experimental evidence in animal groups support our findings that information transfer is anisotropic, arising from the non-reciprocal nature of local vision-based interactions. In rummy-nose tetras, U-turns propagate front-to-back through the school at an approximately constant speed [54], whereas in pigeon flocks, the lateral placement of the eyes biases visual interactions toward side neighbors, leading to predominantly lateral information flow [55]. Assessment of the relative effects of inertia [27] and non-reciprocal visual interactions on the transfer of information in natural animal groups would require integrating models with empirical data [56].

Fragmentation slows down information propagation and merging speeds it up. We next examined splitting events during school self-reorganization. In Fig. 6D, we show trajectories of the splitting event pointed out in Fig. 4E, where the polarized school of $10,000$ swimmers splits into three subgroups, each turning in a different direction. We analyzed each subgroup (Figs. 6D, S5D-F) and found that information travels linearly at nearly the same speed in all three subgroups, at about three fold faster than the self-propelled speed U, but at much slower compared to information travel speed during free turning (Fig. 6F, 7B). This is perhaps not surprising given the loss of spatial correlation prior to and during fragmentation (Fig. 4F,G).

We also examined information transfer during merging events. In Fig. 6G, we show trajectories of a merging event in the simulation of 10,000 swimmers, where two subgroups, starting from polarized states in different directions, turn and merge into a single subgroup. During merging, swimmers from different subgroups do not mix. Analyzing each subgroup (Figs. 6E,F, S5G-I), we found that the information transfer speed increases, reaching up to 40 fold that of the self-propelled speed, much faster than information propagation in free turning and during fragmentation. To further probe the robustness of these results, we analyzed multiple merging events in clusters of different sizes ranging from 1000 to 3000 (Fig. S7). We found that

the information transfer speed is consistently higher during merging, indicating that continuous information input from neighboring clusters increases the speed of information propagation (Fig. 7).

Flow interactions enhance information travel speeds. Lastly, we explored the effect of flow interactions on information travel speed. In Fig. 7D, we fixed the alignment and noise intensities and systematically varied the hydrodynamic intensity I_f from 10^{-4} to 0.05. Results are shown in Fig. 7D inset on a semi-log scale. At small hydrodynamic intensity, the school stays cohesive and the information transfer speed follows closely that predicted by the vision-based alignment model $c \propto \alpha I_a$, where we set $\alpha = \langle \text{VND} \rangle$. However, as I_f increases, the information speed diverges from this model prediction.

To help explain the effect of hydrodynamic interactions on information propagation, we considered how a perturbation in phase φ_i propagates via the fluid medium only (Methods). In the continuum limit, we found that, as in the alignment model, hydrodynamic interactions alone cause information to travel from the front to the back of the school with speed $c \propto I_f/\alpha^2$. However, this flow-based scaling does not correctly predict the information travel speed of the school, because of the non-trivial interplay between vision and hydrodynamic interactions. Indeed, hydrodynamics affects the average distance to Voronoi neighbors $\langle \text{VND} \rangle$ (Figs. S1 and S9D), which in turn affects the information travel speed due to alignment $c \propto \alpha I_a$, where $\alpha = \langle \text{VND} \rangle$. If hydrodynamic coupling between swimmers had no direct effect on c other than through its effect on $\langle \text{VND} \rangle$, we would expect $c/\langle \text{VND} \rangle$ to be independent of I_f; rather, it increases linearly with I_f (Fig. 7D), indicating that hydrodynamic interactions, coupled to vision-based alignment, enhance information transfer speeds.

Discussion

We explored information propagation in mathematical models of massive schools of fish, consisting of up to 50,000 individuals. We showed that (1) as the school size increases, flow interactions

destabilize global polarization, creating locally polarized clusters that dynamically self-organize, fragment and reassemble, akin to empirical observations in natural fish schools [25]; (2) while correlations in velocity fluctuations in cohesive and polarized clusters are scale-free, splitting events are preceded by a decrease in correlation length; (3) information propagates linearly in time within cohesive groups, at speeds exceeding 20 times that of the swimming speed of the individual, thanks to the non-reciprocal nature of visual interactions between individuals, with inertia playing no part in this ballistic information transfer speed; (4) the speed of information propagation is robust to group size but varies with self-organization: merging of separate clusters increases the speed of information transfer within each cluster, while fragmentation decreases it; and (5) flow interactions enhance the information propagation speed.

Our findings have important implications on size regulation [57, 58] and behavioral adaptations [59] in living animal groups. Our model predicts that larger and faster-moving swimmers that generate stronger dipolar flows fragment with increasing number of swimmers, and smaller-sized swimmers can school cohesively in bigger numbers; Indeed, several of the natural species of fish that form massive schools, such as sardines, herring, and anchovies, have relatively small bodylength, not exceeding 30 cm, and typical swimming speeds of 1 to 2 bodylength per second. The prospect that flow physics may have played a role in the evolution and regulation of group size is an exciting direction for future work [20].

Another key area to explore in future work is the role of flow interactions in modulating the spatial dispersal of fish species [60]. In our model, flow interactions cause large schools to disperse in random directions, akin to a 'divide and conquer' strategy, where the group splits up and explores different regions of the space independently before regrouping. Our results are consistent with observations in pelagic fish schools that fragment and rejoin, with many species of fish exhibiting spatial distributions that are skewed toward small sizes with a long tail toward large sizes [25]. Here, we went beyond reporting the fragmentation-rejoining process to proposing a flow-based mechanism that drives, or at least contributes, to this important behavior in natural fish schools. Understanding the factors that influence spatial dispersal patterns is important

because these patterns, in turn, influence numerous processes that are fundamental for the survival of population, such as mate-finding [61–64], disease transmission [65, 66], foraging and prey-detection [30, 67–70], and predator avoidance [71–73].

In natural animal groups preyed upon by faster-moving predators [26], the speed of information propagation within the group is critical to ensure a swift response to predatory threat. Our result that school fragmentation – a strategy thought to confuse predators [13, 74] – comes at the cost of losing scale-free correlation prior to fragmentation and decreasing the information propagation speed within the group, suggests an evolutionary trade-off between maximizing information propagation within the group and creating confusion for the predator. It also suggests that fragmenting the school could be an effective predation strategy that weakens the perception range of the prey, especially in collective predation [75, 76].

Methods

A. Computational method

To numerically solve the system of equations (1-2) for a large number of fish N, one needs a computationally efficient approach to handle the all-to-all hydrodynamic interactions and Voronoi tessellation at each time step. The computational complexity due to the hydrodynamic interactions in (2) scales with $\mathcal{O}(N^2)$. To handle these interactions, we optimized and paralleled the code responsible for computing the direct sum in (2) using a just-in-time compiler called *Numba* [77]. *Numba* compiles, optimizes, and parallelizes the Python code to approach the computational performance of C or Fortran. Note that fast multipole methods (FMM) reduce the computational complexity of the hydrodynamic interactions from $\mathcal{O}(N^2)$ to nearly $\mathcal{O}(N)$ [78, 79], but FMM algorithms do not have a significant advantage over direct sum in systems of the order of 10^4 agents [79], hence our choice to directly optimize the $\mathcal{O}(N^2)$ sum in (2). For the Voronoi tessellation in two dimensions (2D), efficient algorithms exist for reducing this task to $\mathcal{O}(N \log N)$ [80]. We utilized the function `Delaunay` in *Scipy* [81]. We implemented these approaches in evaluating the right-hand sides of (1) at each time step dt, discretized the noise term using $dW_t = \mathcal{N}(0,1)\sqrt{dt}$, and used an explicit Euler–Maruyama method to integrate (1) forward in time at a timestep size $dt = 10^{-2}$ [82]. We run our algorithm on an Exxact Valence Workstation with a 56-core Intel Xeon W9-3495X CPU. With this software and hardware setup, a timestep takes about 1 second for $10,000$ agents, with hydrodynamic interactions and Voronoi tessellation taking about half of the computational time each. Integrating

the motion of $10,000$ agents over a time interval $T = 1000$ took about a day; integrating the motion of $50,000$ swimmers for the same time interval took about three weeks.

B. Statistical and data-driven analysis

Polar order parameter. To quantify the degree of polarization within each group or subgroup of swimmers, we calculated the polar order parameter $P = \| \sum_{j=1}^{N} \mathbf{p}_j \| / N \in [0, 1]$, where $P = 1$ when all swimmers are heading in the same direction; it is nearly zero for randomly oriented swimmers.

Identifying splitting and merging events Fish remained cohesive in relatively small groups, but in large schools, we observed dynamic splitting and merging where the large school got divided into subgroups, each moving in a different direction that seemed to randomly rejoin and divide again for the entire simulation time. To identify these splitting and merging events, we examined the time evolution of the polar order parameter: P rapidly decreased or increased when a splitting or merging event occurred. To determine the time scale at which these events took place, we calculated the dominant frequency of dP/dt using Fast Fourier transformation (FFT). In the absence of splitting and merging events, such as at small number of fish, the FFT is characterized by high frequencies due to individual-level noise. We discarded these frequencies (equivalent to a low-pass filter) to identify the frequencies at which the splitting and merging events occurred in large schools. We discard all frequencies larger than 0.5. The inverse of this dominant frequency defines the time scale of splitting and merging.

Clustering algorithm. To identify the number of distinct subgroups in large groups of swimmers as a function of time, we used a numerical approach based on clustering methods [83]. Because in this active system, the individual clusters have versatile and time-varying shapes, we needed a computational approach that could handle arbitrarily shaped clusters. Classic clustering methods based on expectation–maximization algorithms [84], such as K-means [85] or Mixture Models [86], suffer in identifying intertwined clusters with time-varying shapes. Here, we used density-based methods that are designed to separate low- and high-density regimes in the domain and identify complex-shaped clusters [49–51, 87, 88]; particularly, we used the Hierarchical Density-Based Spatial Clustering of Applications with Noise (HDBSCAN) algorithm [49–51], implemented in the *scikit-learn* package [89], which has been successfully applied to identify clusters in simulations of the Vicsek model [83].

Spatial correlation in velocity fluctuations. The degree of polarization P provides little insights into the collective response in a school [1, 52]. To understand the collective response, we examined how fluctuations in each swimmer's velocity correlate with those of others. For swimmer i, we defined the fluctuation $\delta\mathbf{v}_i$ around the group's mean velocity as $\delta\mathbf{v}_i = \mathbf{v}_i - \langle\mathbf{v}\rangle_N$, where $\langle\mathbf{v}\rangle_N = \sum_{j=1}^{N} \mathbf{v}_j / N$. By construction, $\sum_{i=1}^{N} \delta\mathbf{v}_i = 0$, which simply indicates no net motion in the center of mass reference frame of the school. We defined the spatial

correlation function $C(\mathbf{r})$ of fluctuations, which measures the average inner product of velocity fluctuations of swimmers at a distance r from each other,

$$C(r) = \frac{1}{C_o} \frac{\sum_i \sum_j (\delta \mathbf{v}_i \cdot \delta \mathbf{v}_j) \delta(r - r_{ij})}{\sum_i \sum_j \delta(r - r_{ij})}. \tag{5}$$

Here, the Dirac-delta function $\delta(r - r_{ij})$, where $r_{ij} = \|\mathbf{r}_{ij}\|$ and $\mathbf{r}_{ij} = \mathbf{x}_i - \mathbf{x}_j$, selects pairs of swimmers at mutual distance r, and C_o is a normalization factor such that $C(r = 0) = 1$.

Time delays during turning and information propagation within the group. When a cohesive polarized group of swimmers performed a collective turn, to define the turn, we examined the time evolution of the curvature $\kappa_i = \frac{\|\mathbf{v}_i \times \dot{\mathbf{v}}_i\|}{\|\mathbf{v}_i\|^3}$ of the trajectory traced by swimmer i, where $\dot{\mathbf{v}}_i$ is the swimmer's acceleration. In 2D, the curvature can be calculated directly in terms of the time derivatives of the coordinates (x_i, y_i), namely, $k_i(t) = \frac{\dot{x}_i \ddot{y}_i - \dot{y}_i \ddot{x}_i}{(\dot{x}_i^2 + \dot{y}_i^2)^{3/2}}$. The time-evolution of the curvature $\kappa_i(t)$ of a swimmer i undergoing a turn exhibits a maximum at the time of the turn. Inspired by [27, 90], and given two swimmers i and j, we defined the mutual turning delay τ_{ij} as the time required to shift the full curve of $\kappa_j(t)$ to maximally overlap it with $\kappa_i(t)$

$$\tau_{ij} = \underset{\tau}{\text{argmax}} \int_{t=t_1}^{t_2} k_i(t) k_j(t - \tau) dt. \tag{6}$$

Here, $\tau_{ij} < 0$ means fish i turns ahead of fish j and vice versa. In the absence of noise, time ordering requires that $\tau_{ij} = \tau_{ik} + \tau_{kj}$, for each triplet i, j, k. For example, if i turns 10 time units before k, and k turns 5 time units before j, then i turns 15 time units before j. Because we are dealing with a noisy system, this equality may not be strictly satisfied, but τ_{ij} is equal to $\tau_{ik} + \tau_{kj}$ on average.

We next ranked the group of fish undergoing a turn based on their time of maximal curvature. For each fish i, we calculated how many other fish it has turned ahead of [27, 91]. The order of this number – the number of other fish a fish precedes in turning – defines a rank for the fish; the first-ranked fish is ahead of the largest number of fish and its turning time is used to set the time t_1 of the onset of the turning event. In a perfect system, with no noise, the turning time t_i of a lagging fish i can be calculated directly relative to the turning time of the first-ranked fish 1, $t_i = t_1 + \tau_{i1}$. However, because the system is noisy, this method of calculating t_i introduces small statistical errors. To minimize these errors, we define t_i using the mutual delay τ_{ij} with respect to all swimmers j ranked higher than i,

$$t_i = \frac{1}{\text{rank}_i - 1} \sum_{\text{rank}_j < \text{rank}_i} (t_i + \tau_{ij}), \qquad i > 1 \tag{7}$$

C. Coarse-grained analysis of information propagation

Alignment model. Starting from the microscopic equation describing the time evolution of swimmer's heading

$$\dot{\theta}_i = I_a \frac{\sum_{j\in\mathcal{N}_i} \sin\phi_{ij}(1+\gamma\cos\theta_{ij})}{\sum_{j\in\mathcal{N}_i}(1+\gamma\cos\theta_{ij})}, \tag{8}$$

where $\gamma \in [0,1]$ is a parameter that controls the strength of vision-based bias, or non-reciprocity, toward neighbors in front: $\gamma = 1$ is used in (1) while $\gamma = 0$ means no visual bias. We derive a continuum equation under the following conditions. Firstly, we consider a highly polarized school, which means that the orientation of each swimmer within the school can be decomposed into the average heading direction of the school $\langle\theta\rangle$ and a small fluctuation φ_i of individual swimmers i about the average heading θ, namely $\theta_i = \langle\theta\rangle + \varphi_i$. Without loss of generality, we assume the $\langle\theta\rangle = 0$, which aligns the positive x-direction with the moving direction of the group. Based on this assumption, $\sin\phi_{ij} = \sin(\theta_j - \theta_i) = \sin(\varphi_j - \varphi_i) \approx \varphi_j - \varphi_i$, and $\cos\theta_{ij} = \cos(\arctan\frac{y_j-y_i}{x_j-x_i} - \theta_i) = \cos(\arctan\frac{y_j-y_i}{x_j-x_i} - \varphi_i)$. Substitute these relationships into (1), we get

$$\frac{\partial\varphi_i}{\partial t} = \frac{I_a}{N}\sum_{j\in\mathcal{N}_i}(\varphi_j - \varphi_i)\left[1+\gamma\cos(\arctan\frac{y_j-y_i}{x_j-x_i} - \varphi_i)\right], \tag{9}$$

Secondly, we assume that the swimmers are located on a 2d lattice of mesh size α, and mesh orientation aligned with the swimming direction. We aim to coarse-grain the discrete equations (1) over a coarse-graining box containing a focal swimmer and four immediate neighbors, such that a swimmer i responds to its direct front, left, back, and right neighbors, indexed by $i1$, $i2$, $i3$, $i4$. Their locations with respect to particle i can be written as $\mathbf{x}_{i1} - \mathbf{x}_i = (\alpha, 0)$, $\mathbf{x}_{i2} - \mathbf{x}_i = (0, \alpha)$, $\mathbf{x}_{i3} - \mathbf{x}_i = (-\alpha, 0)$, and $\mathbf{x}_{i4} - \mathbf{x}_i = (0, -\alpha)$. Plug it into (9) and reorganize to arrive at

$$\frac{\partial\varphi_i}{\partial t} = \frac{\alpha^2 I_a}{4}\left(\frac{\varphi_{i1}+\varphi_{i3}-2\varphi_i}{\alpha^2} + \frac{\varphi_{i2}+\varphi_{i4}-2\varphi_i}{\alpha^2}\right) + \frac{\gamma\alpha I_a}{2}\left(\cos\varphi_i\frac{\varphi_{i1}-\varphi_{i3}}{2\alpha} + \sin\varphi_i\frac{\varphi_{i2}-\varphi_{i4}}{2\alpha}\right) \tag{10}$$

The finite difference can be approximated by first-order and second-order derivatives, such that at small φ where $\cos\varphi \sim 1$, $\sin\varphi \sim \varphi$, we arrive at

$$\frac{\partial\varphi}{\partial t} = \frac{\alpha^2 I_a}{4}\Delta\varphi + \frac{\gamma\alpha I_a}{2}\left(\frac{\partial\varphi}{\partial x} + \varphi\frac{\partial\varphi}{\partial y}\right) \tag{11}$$

The equation governing ϕ has an anisotropic advection term, where ϕ is advected linearly in the longitudinal direction x and non-linearly, albeit at much smaller speed (considering that $\varphi \ll 1$) in the transverse direction. Ignoring the nonlinear term, we get

$$\frac{\partial\varphi}{\partial t} = \frac{\alpha^2 I_a}{4}\Delta\varphi + \frac{\gamma\alpha I_a}{2}\frac{\partial\varphi}{\partial x}. \tag{12}$$

The diffusion term scales with $\alpha^2 I_a$, while the advection term scales with αI_a, implying that in dense schools, linear advection is dominant. Ignoring diffusion and considering an initial perturbation in the longitudinal x-direction of form $\varphi_0(x,y) = A\sin(k_x x)$, the perturbation propagates from front to back at a speed $c = \gamma\alpha I_a/2$,

$$\varphi(t,x,y) = A\sin(k_x(x+ct)). \tag{13}$$

Hydrodynamic interaction model. Considering the group is heading in the same direction and ignoring noise and all vision-based interactions in (1), a small perturbation in φ_i about the heading direction propagates via hydrodynamic interactions only following the simpler equation

$$\frac{\partial\varphi_i}{\partial t} = \mathbf{p}_i \cdot \frac{d\mathbf{U}_i}{d\mathbf{x}}|_{\mathbf{x}_i} \cdot \mathbf{p}_i^{\perp}. \tag{14}$$

Here, to simply the analysis, we consider the swimmers to form an infinite one-dimensional lattice with equally-spaced potential dipoles of mesh size α, such that the flow field at location i is given by [33],

$$\mathbf{U}_i = \sum_{j=-\infty, j\neq i}^{\infty} \frac{I_f}{\pi}\frac{\mathbf{p}_j^{\perp}\sin 2\theta_{ji} + \mathbf{p}_j\cos 2\theta_{ji}}{r_{ij}^2} \tag{15}$$

Considering perturbations of wavenumber k and associated wavelength $2\pi/k = (K-1)\alpha$, where K is the perturbed number of swimmers, we employ the analytical expression derived in [33], which transforms the infinite summation in (15) to a finite summation. Substituting back into (14), we get

$$\frac{\partial\varphi_i}{\partial t} = \frac{-2\pi^2 I_f}{K^3\alpha^3}\sum_{j=1, j\neq i}^{K}\frac{\cos\left[\pi(i-j)/K\right]}{\sin^3\left[\pi(i-j)/K\right]}\sin(\varphi_j - 2\varphi_i) \tag{16}$$

Linearizing using $\sin(\varphi_j - 2\varphi_i) \approx \varphi_j - 2\varphi_i$, and approximating the finite difference by first-order derivatives, we arrive at

$$\frac{\partial\varphi}{\partial t} = \frac{2I_f k}{\pi\alpha}\frac{\partial\varphi}{\partial x}\int_{\alpha}^{\pi/2}\frac{x\cos x}{\sin^3 x}dx, \tag{17}$$

where the integral is a constant depends only on wave number k. This shows that perturbations propagate linearly while getting amplified by hydrodynamic interactions.

Data Availability

The sample data generated in this study have been deposited in GitHub under accession code `https://github.com/ekanso/schooling_extreme`. Source data are provided as a Source Data file.

Code Availability

Code is openly available on GitHub at `https://github.com/ekanso/schooling_extreme`.

References

1. Cavagna, A. *et al.* Scale-free correlations in starling flocks. *Proceedings of the National Academy of Sciences* **107,** 11865–11870 (2010).

2. Bialek, W. *et al.* Statistical mechanics for natural flocks of birds. *Proceedings of the National Academy of Sciences* **109,** 4786–4791 (2012).

3. Mora, T. *et al.* Local equilibrium in bird flocks. *Nature physics* **12,** 1153–1157 (2016).

4. Couzin, I. D., Krause, J., James, R., Ruxton, G. D. & Franks, N. R. Collective memory and spatial sorting in animal groups. *Journal of theoretical biology* **218,** 1–11 (2002).

5. Couzin, I. D., Krause, J., Franks, N. R. & Levin, S. A. Effective leadership and decision-making in animal groups on the move. *Nature* **433,** 513–516 (2005).

6. Gautrais, J. *et al.* Deciphering Interactions in Moving Animal Groups. *PLOS Computational Biology* **8,** 1–11. `https://doi.org/10.1371/journal.pcbi.1002678` (Sept. 2012).

7. Garnier, S., Gautrais, J. & Theraulaz, G. The biological principles of swarm intelligence. *Swarm intelligence* **1,** 3–31 (2007).

8. Cavagna, A. *et al.* Dynamic scaling in natural swarms. *Nature Physics* **13,** 914–918 (2017).

9. Sayin, S. *et al.* The behavioral mechanisms governing collective motion in swarming locusts. *Science* **387,** 995–1000. eprint: `https://www.science.org/doi/pdf/10.1126/science.adq7832`. `https://www.science.org/doi/abs/10.1126/science.adq7832` (2025).

10. Vicsek, T., Czirók, A., Ben-Jacob, E., Cohen, I. & Shochet, O. Novel type of phase transition in a system of self-driven particles. *Physical review letters* **75,** 1226 (1995).

11. Toner, J. & Tu, Y. Long-range order in a two-dimensional dynamical XY model: how birds fly together. *Physical review letters* **75,** 4326 (1995).

12. Toner, J. & Tu, Y. Flocks, herds, and schools: A quantitative theory of flocking. *Physical review E* **58,** 4828 (1998).

13. Couzin, I. D., Krause, J., *et al.* Self-organization and collective behavior in vertebrates. *Advances in the Study of Behavior* **32,** 10–1016 (2003).

14. Aranson, I. S. & Tsimring, L. S. Patterns and collective behavior in granular media: Theoretical concepts. *Reviews of modern physics* **78,** 641–692 (2006).

15. Calovi, D. S. *et al.* Swarming, schooling, milling: phase diagram of a data-driven fish school model. *New journal of Physics* **16,** 015026 (2014).

16. Filella, A., Nadal, F., Sire, C., Kanso, E. & Eloy, C. Model of collective fish behavior with hydrodynamic interactions. *Physical review letters* **120,** 198101 (2018).

17. Huang, C., Ling, F. & Kanso, E. Collective phase transitions in confined fish schools. *Proceedings of the National Academy of Sciences* **121,** e2406293121 (2024).

18. Heydari, S., Hang, H. & Kanso, E. Mapping Spatial Patterns to Energetic Benefits in Groups of Flow-coupled Swimmers. *Elife,* 2024–02 (2024).

19. Peterson, A. N., Swanson, N. & McHenry, M. J. Fish communicate with water flow to enhance a school's social network. *Journal of Experimental Biology* **227** (2024).

20. Rieucau, G., Fernö, A., Ioannou, C. C. & Handegard, N. O. Towards of a firmer explanation of large shoal formation, maintenance and collective reactions in marine fish. *Reviews in Fish Biology and Fisheries* **25,** 21–37 (2015).

21. Calovi, D. S. *et al.* Disentangling and modeling interactions in fish with burst-and-coast swimming reveal distinct alignment and attraction behaviors. *PLoS computational biology* **14,** e1005933 (2018).

22. Anderson, P. W. More Is Different: Broken symmetry and the nature of the hierarchical structure of science. *Science* **177,** 393–396 (1972).

23. Strogatz, S. *et al.* Fifty years of 'More is different'. *Nature Reviews Physics* **4,** 508–510 (2022).

24. Partridge, B. L. Internal dynamics and the interrelations of fish in schools. *Journal of comparative physiology* **144,** 313–325 (1981).

25. Niwa, H.-S. School size statistics of fish. *Journal of theoretical biology* **195,** 351–361 (1998).

26. Rieucau, G., De Robertis, A., Boswell, K. & Handegard, N. School density affects the strength of collective avoidance responses in wild-caught Atlantic herring Clupea harengus: a simulated predator encounter experiment. *Journal of Fish Biology* **85,** 1650–1664 (2014).

27. Attanasi, A. *et al.* Information transfer and behavioural inertia in starling flocks. *Nature physics* **10,** 691–696 (2014).

28. Nagy, M., Ákos, Z., Biro, D. & Vicsek, T. Hierarchical group dynamics in pigeon flocks. *Nature* **464,** 890–893 (2010).

29. Ioannou, C. C., Couzin, I. D., James, R., Croft, D. P. & Krause, J. Social organisation and information transfer in schooling fish. *Fish cognition and behavior* **2,** 217–239 (2011).

30. Handegard, N. O. *et al.* The dynamics of coordinated group hunting and collective information transfer among schooling prey. *Current biology* **22,** 1213–1217 (2012).

31. Cheng Hou Tsang, A. & Kanso, E. Flagella-induced transitions in the collective behavior of confined microswimmers. *Phys. Rev. E* **90,** 021001. `https://link.aps.org/doi/10.1103/PhysRevE.90.021001` (2 Aug. 2014).

32. Tsang, A. C. H. & Kanso, E. Density shock waves in confined microswimmers. *Physical review letters* **116,** 048101 (2016).

33. Tsang, A. C. H., Shelley, M. J. & Kanso, E. Activity-induced instability of phonons in 1D microfluidic crystals. *Soft Matter* **14,** 945–950 (2018).

34. Tsang, A. C. H. & Kanso, E. Dipole interactions in doubly periodic domains. *Journal of Nonlinear Science* **23,** 971–991 (2013).

35. Zhu, X., He, G. & Zhang, X. Flow-Mediated Interactions between Two Self-Propelled Flapping Filaments in Tandem Configuration. *Physical Review Letters* **113,** 238105. ISSN: 0031-9007 (2014).

36. Newbolt, J. W. *et al.* Flow interactions lead to self-organized flight formations disrupted by self-amplifying waves. *Nature communications* **15,** 3462 (2024).

37. Engelmann, J., Hanke, W., Mogdans, J. & Bleckmann, H. Hydrodynamic stimuli and the fish lateral line. *Nature* **408,** 51–52. https://doi.org/10.1038/35040706 (2000).

38. Ristroph, L., Liao, J. C. & Zhang, J. Lateral line layout correlates with the differential hydrodynamic pressure on swimming fish. *Physical Review Letters* **114,** 018102 (2015).

39. Colvert, B. & Kanso, E. Fishlike rheotaxis. *Journal of Fluid Mechanics* **793,** 656–666 (2016).

40. Ashraf, I. *et al.* Simple phalanx pattern leads to energy saving in cohesive fish schooling. *Proc. Nat. Acad. Sci.* **114,** 9599–9604. ISSN: 10916490 (2017).

41. Zhang, P., Krasner, E., Peterson, S. D. & Porfiri, M. An information-theoretic study of fish swimming in the wake of a pitching airfoil. *Physica D: Nonlinear Phenomena* **396,** 35–46 (2019).

42. Li, L. *et al.* Vortex phase matching as a strategy for schooling in robots and in fish. *Nature Communications* **11,** 5408 (2020).

43. McKee, A., Soto, A. P., Chen, P. & McHenry, M. J. The sensory basis of schooling by intermittent swimming in the rummy-nose tetra (Hemigrammus rhodostomus). *Proceedings of the Royal Society B* **287,** 20200568 (2020).

44. Zheng, Z., Tao, Y., Xiang, Y., Lei, X. & Peng, X. Body orientation change of neighbors leads to scale-free correlation in collective motion. *Nature Communications* **15,** 8968 (2024).

45. Avni, Y., Fruchart, M., Martin, D., Seara, D. & Vitelli, V. The non-reciprocal Ising model. *arXiv preprint arXiv:2311.05471* (2023).

46. Fruchart, M., Hanai, R., Littlewood, P. B. & Vitelli, V. Non-reciprocal phase transitions. *Nature* **592,** 363–369 (2021).

47. Kanso, E. & Tsang, A. C. H. Dipole models of self-propelled bodies. *Fluid Dynamics Research* **46,** 061407 (2014).

48. Wiener, N. *Norbert Wiener: Collected Works* (MIT Press Cambridge, Mass., 1976).

49. Ester, M., Kriegel, H.-P., Sander, J. & Xu, X. *A density-based algorithm for discovering clusters in large spatial databases with noise* in (AAAI Press, Portland, Oregon, 1996), 226–231.

50. Campello, R. J. G. B., Moulavi, D. & Sander, J. *Density-Based Clustering Based on Hierarchical Density Estimates* in *Pacific-Asia Conference on Knowledge Discovery and Data Mining* (2013). https://api.semanticscholar.org/CorpusID:32384865.

51. McInnes, L. & Healy, J. *Accelerated hierarchical density based clustering* in *2017 IEEE international conference on data mining workshops (ICDMW)* (2017), 33–42.

52. Cavagna, A., Giardina, I. & Grigera, T. S. The physics of flocking: Correlation as a compass from experiments to theory. *Physics Reports* **728,** 1–62 (2018).

53. National Academies of Sciences, E. & Medicine. *Physics of Life* ISBN: 978-0-309-27400-5. https://nap.nationalacademies.org/catalog/26403/physics-of-life (The National Academies Press, Washington, DC, 2022).

54. Lecheval, V. *et al.* Social conformity and propagation of information in collective U-turns of fish schools. *Proceedings of the Royal Society B: Biological Sciences* **285,** 20180251 (2018).

55. Chen, D., Liu, X., Xu, B. & Zhang, H.-T. Intermittence and connectivity of interactions in pigeon flock flights. *Scientific reports* **7,** 10452 (2017).

56. Rosenthal, S. B., Twomey, C. R., Hartnett, A. T., Wu, H. S. & Couzin, I. D. Revealing the hidden networks of interaction in mobile animal groups allows prediction of complex behavioral contagion. *Proceedings of the National Academy of Sciences* **112,** 4690–4695 (2015).

57. Higashi, M. & Yamamura, N. What determines animal group size? Insider-outsider conflict and its resolution. *The American Naturalist* **142,** 553–563 (1993).

58. Bonabeau, E., Dagorn, L. & FREon, P. Scaling in animal group-size distributions. *Proceedings of the National Academy of Sciences* **96,** 4472–4477 (1999).

59. Roberts, G. Why individual vigilance declines as group size increases. *Animal behaviour* **51,** 1077–1086 (1996).

60. Bowler, D. E. & Benton, T. G. Causes and consequences of animal dispersal strategies: relating individual behaviour to spatial dynamics. *Biological reviews* **80,** 205–225 (2005).

61. Cardé, R. T. & Mafra-Neto, A. in *Insect pheromone research* 275–290 (Springer, 1997).

62. Huang, Y., Yen, J. & Kanso, E. Detection and tracking of chemical trails in bio-inspired sensory systems. *European Journal of Computational Mechanics* **26,** 98–114 (2017).

63. Hang, H., Jiao, Y., Merel, J. & Kanso, E. Flow currents support simple and versatile trail-tracking strategies. *Phys. Rev. Res.*, –. `https://link.aps.org/doi/10.1103/qj9q-p7rg` (July 2025).

64. Jiao, Y., Hang, H., Merel, J. & Kanso, E. Sensing flow gradients is necessary for learning autonomous underwater navigation. *Nature Communication* (2025).

65. Kent, M. L. *et al.* Recommendations for control of pathogens and infectious diseases in fish research facilities. *Comparative Biochemistry and Physiology Part C: Toxicology & Pharmacology* **149,** 240–248 (2009).

66. Mittal, R., Ni, R. & Seo, J.-H. The flow physics of COVID-19. *Journal of fluid Mechanics* **894,** F2 (2020).

67. Pohlmann, K., Grasso, F. W. & Breithaupt, T. Tracking wakes: the nocturnal predatory strategy of piscivorous catfish. *Proceedings of the National Academy of Sciences* **98,** 7371–7374 (2001).

68. Berdahl, A., Torney, C. J., Ioannou, C. C., Faria, J. J. & Couzin, I. D. Emergent sensing of complex environments by mobile animal groups. *Science* **339,** 574–576 (2013).

69. Basil, J. & Atema, J. Lobster orientation in turbulent odor plumes: simultaneous measurement of tracking behavior and temporal odor patterns. *The Biological Bulletin* **187,** 272–273 (1994).

70. Weissburg, M. J. & Zimmer-Faust, R. K. Odor plumes and how blue crabs use them in finding prey. *Journal of Experimental Biology* **197,** 349–375 (1994).

71. Radakov, D. V. *Schooling in the ecology of fish* eng. ISBN: 0706513517 (J. Wiley, New York, 1973).

72. Gerlotto, F., Bertrand, S., Bez, N. & Gutierrez, M. Waves of agitation inside anchovy schools observed with multibeam sonar: a way to transmit information in response to predation. *ICES Journal of Marine Science* **63,** 1405–1417 (2006).

73. Jiao, Y., Colvert, B., Man, Y., McHenry, M. J. & Kanso, E. Evaluating evasion strategies in zebrafish larvae. *Proceedings of the National Academy of Sciences* **120,** e2218909120 (2023).

74. Humphries, D. & Driver, P. Protean defence by prey animals. *Oecologia* **5,** 285–302 (1970).

75. Angelani, L. Collective predation and escape strategies. *Physical review letters* **109,** 118104 (2012).

76. Papadopoulou, M., Hildenbrandt, H., Sankey, D. W., Portugal, S. J. & Hemelrijk, C. K. Self-organization of collective escape in pigeon flocks. *PLoS computational biology* **18,** e1009772 (2022).

77. Lam, S. K., Pitrou, A. & Seibert, S. *Numba: A llvm-based python jit compiler* in *Proceedings of the Second Workshop on the LLVM Compiler Infrastructure in HPC* (2015), 1–6.

78. Greengard, L. & Rokhlin, V. A fast algorithm for particle simulations. *Journal of computational physics* **73,** 325–348 (1987).

79. Ying, L., Biros, G. & Zorin, D. A kernel-independent adaptive fast multipole algorithm in two and three dimensions. *Journal of Computational Physics* **196,** 591–626 (2004).

80. Barber, C. B., Dobkin, D. P. & Huhdanpaa, H. The quickhull algorithm for convex hulls. *ACM Transactions on Mathematical Software (TOMS)* **22,** 469–483 (1996).

81. Virtanen, P. *et al.* SciPy 1.0: Fundamental Algorithms for Scientific Computing in Python. *Nature Methods* **17,** 261–272 (2020).

82. Kloeden, P. E., Platen, E., Kloeden, P. E. & Platen, E. *Stochastic differential equations* (Springer, 1992).

83. Miyahara, H., Yoneki, H. & Roychowdhury, V. Vicsek Model Meets DBSCAN: Cluster Phases in the Vicsek Model. *arXiv preprint arXiv:2307.12538* (2023).

84. Dempster, A. P., Laird, N. M. & Rubin, D. B. Maximum likelihood from incomplete data via the EM algorithm. *Journal of the royal statistical society: series B (methodological)* **39,** 1–22 (1977).

85. MacQueen, J. *Some methods for classification and analysis of multivariate observations* in *Proceedings of 5-th Berkeley Symposium on Mathematical Statistics and Probability/University of California Press* (1967).

86. Duda, R. O. & Hart, P. E. *Pattern classification and scene analysis* in *A Wiley-Interscience publication* (1974). `https://api.semanticscholar.org/CorpusID:12946615`.

87. Schubert, E., Sander, J., Ester, M., Kriegel, H. P. & Xu, X. DBSCAN revisited, revisited: why and how you should (still) use DBSCAN. *ACM Transactions on Database Systems (TODS)* **42,** 1–21 (2017).

88. Kang, C.-P. *et al.* An automatic method to calculate heart rate from zebrafish larval cardiac videos. *BMC bioinformatics* **19,** 1–10 (2018).

89. Pedregosa, F. *et al.* Scikit-learn: Machine learning in Python. *the Journal of machine Learning research* **12,** 2825–2830 (2011).

90. Attanasi, A. *et al.* Emergence of collective changes in travel direction of starling flocks from individual birds' fluctuations. *Journal of The Royal Society Interface* **12,** 20150319 (2015).

91. Cavagna, A. & Giardina, I. Bird flocks as condensed matter. *Annu. Rev. Condens. Matter Phys.* **5,** 183–207 (2014).

92. Student. The probable error of a mean. *Biometrika,* 1–25 (1908).

93. Fisher, R. A. On the interpretation of χ 2 from contingency tables, and the calculation of P. *Journal of the royal statistical society* **85,** 87–94 (1922).

Acknowledgement

Funding support provided by the NSF grants RAISE IOS-2034043 and CBET-2100209, ONR grants N00014-22-1-2655 and N00014-19-1-2035, and NIH grant R01-HL153622 (all to E.K.). E.K. is grateful to Andrea Cavagna for a helpful discussion.

Author Contributions Statement

E.K. conceptualized and supervised the research; H.H. and C.H. wrote code with input from A.B.; H.H. performed simulations and collected data; H.H. and E.K. analyzed the data and prepared figures; E.K. wrote the manuscript and all authors edited and approved it.

Competing Interests Statement

The authors declare no competing interests.

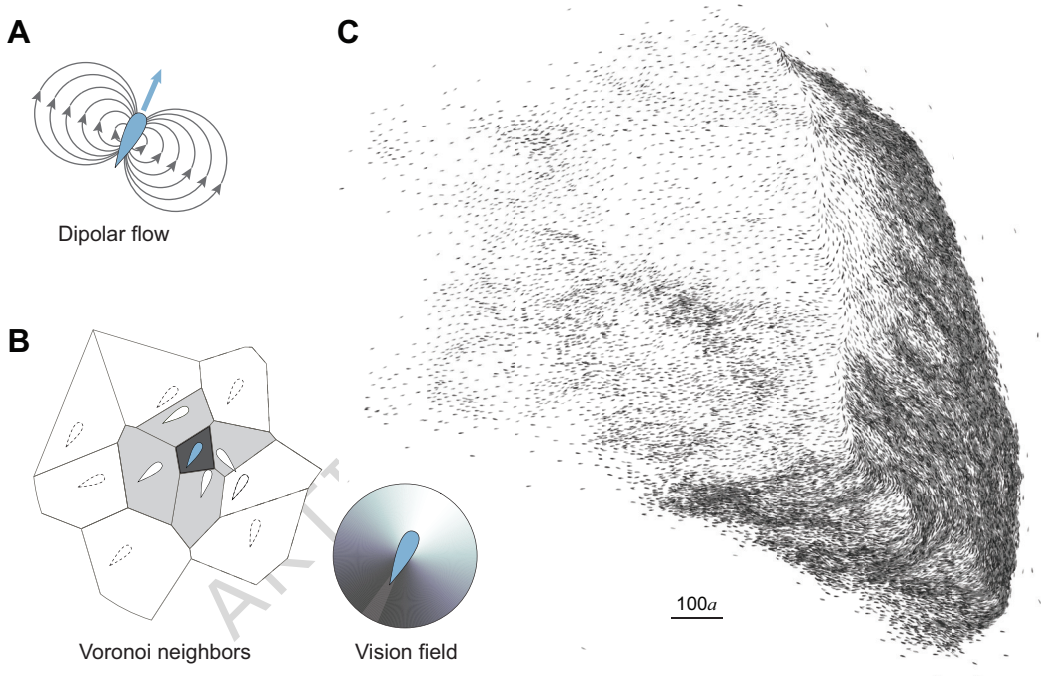

Figure 1: **Emergent behavior in a school of 50,000 fish.** An individual swimmer **A.** creates a dipolar flow disturbance, with dipole intensity proportional to its speed and cross-sectional area, and **B.** responds by turning towards and aligning with its first-level Voronoi neighbors, highlighted in grey in this sample Voronoi tesselation. The individual response is mediated by an asymmetric visual field with frontal bias. **C.** School organizes into coherent polarized clusters that dynamically split and merge, exhibiting large density fluctuations, as shown here in a massive merging event involving about 20% of the fish. In all simulations, total integration time: $T = 1000$. Parameter values: $I_a = 9$, $I_n = 0.5$, $I_f = 0.01$, and $N = 50{,}000$. Suppl. Movie 1.

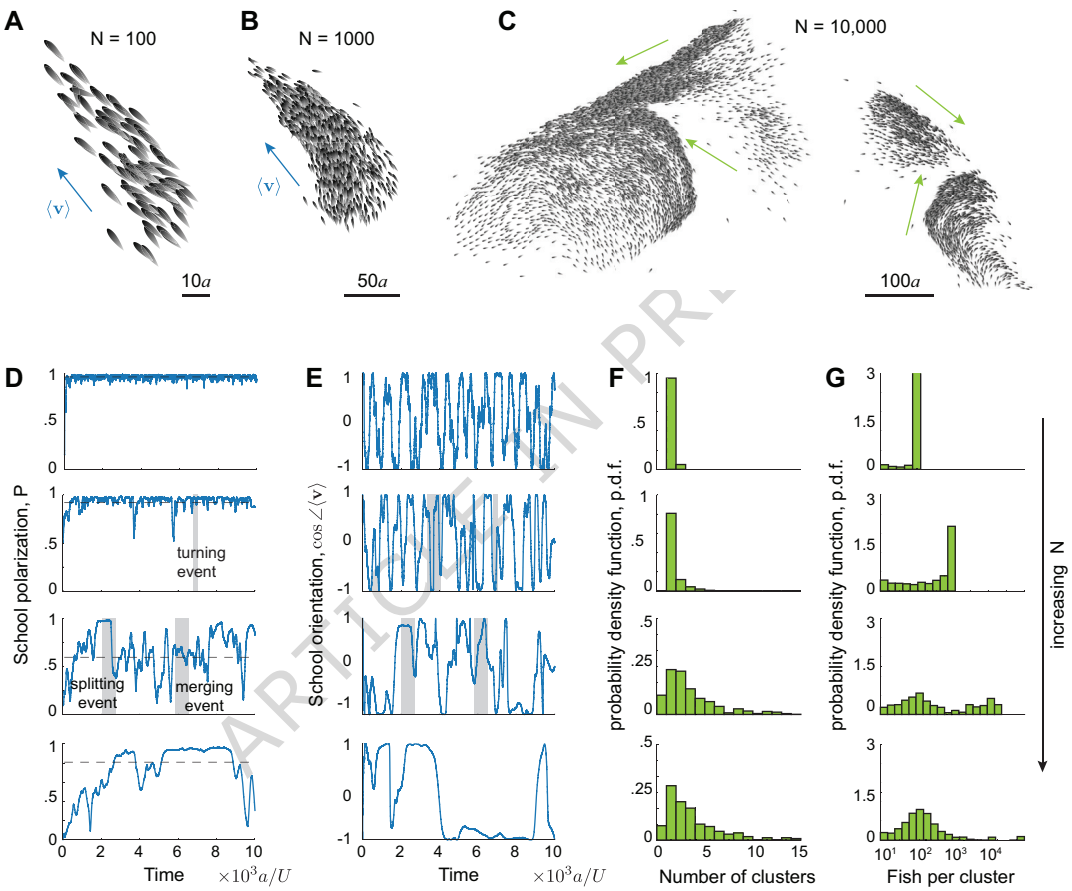

Figure 2: **More is different: self-organized behavior depends on group size.** Snapshots of three schools of **A.** 100, **B.** 1000, and **C.** 10,000 fish. For N=100 and 1000, the school is globally polarized and remains coherent in time, while for N = 10,000, the school continuously reorganizes, dynamically splitting and merging. Blue arrows indicate the school's average velocity, and green arrows indicate the average velocity of each cluster. Time evolution of **D.** school polarization P and **E.** average orientation $\cos\angle\langle\mathbf{v}\rangle$. Distributions of **F.** number of clusters and **G.** number of fish per cluster shown in log scale. Parameter values: $I_a = 9$, $I_n = 0.5$, $I_f = 0.01$. In D-G, from top to bottom, N = 100 1000, 10,000, and 50,000. See Suppl. Movies 1 & 2.

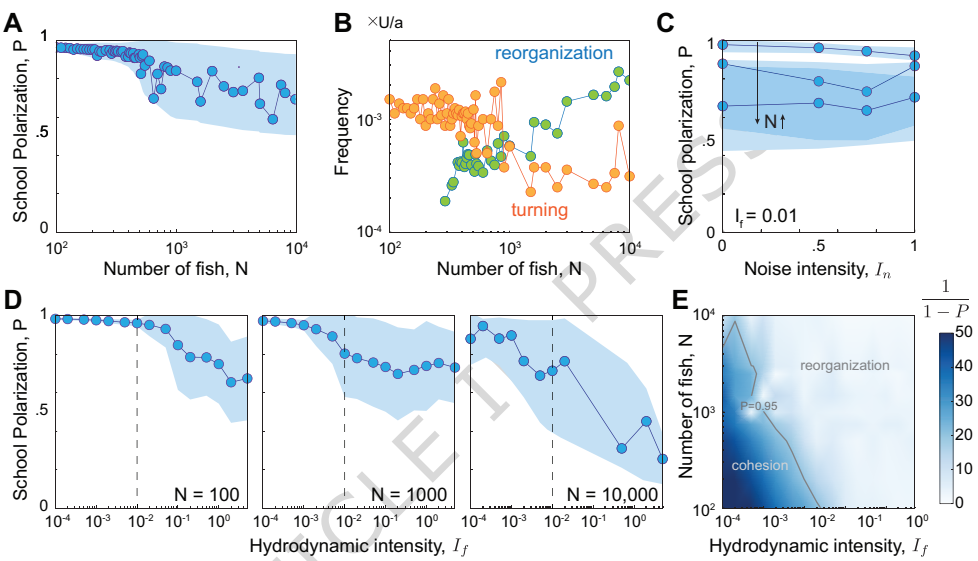

Figure 3: **School cohesiveness depends on the hydrodynamic intensity of individual swimmers.** **A.** time-averaged polarization P versus school size N indicates a transition from a highly-polarized cohesive regime to a regime of constant dynamic organization beyond a critical group size; shaded area indicates standard deviation of P within time series; P is averaged over the last 80% of the simulation time, discounting the initial 20% to eliminate transient effects. **B.** Dominant frequency of dP/dt and $\cos\angle\langle\mathbf{v}\rangle$ versus school size show an increasing frequency of splitting and merging, reflected by sharper changes in dP/dt, with increasing N. In A-B, hydrodynamic intensity is set to $I_f = 0.01$; average school density, nearest neighbor distance, and Voronoi neighbor distance are shown in Fig. S1; corresponding analysis without hydrodynamic interactions ($I_f = 0$) are shown in Fig. S2. Time-averaged polar order parameter P and standard deviation as a function of **C.** noise intensity I_n and **D.** hydrodynamic intensity I_f for schools of size N =100, N =1000, and N =10,000. **E.** Instead of P, we plot $1/(1-P)$ to enhance the contrast of the colormap over the space of hydrodynamic intensity I_f and number of swimmer N. Results show loss of cohesion with increasing N and I_f. Parameter values: $I_a = 9$, $I_n = 0.5$. In **A.**, **C.**, and **D.**, all data points are for mean value over time and Monta Carlo simulations, and transparent box shows the standard deviation. Number of Monte Carlo simulations in Table S1.

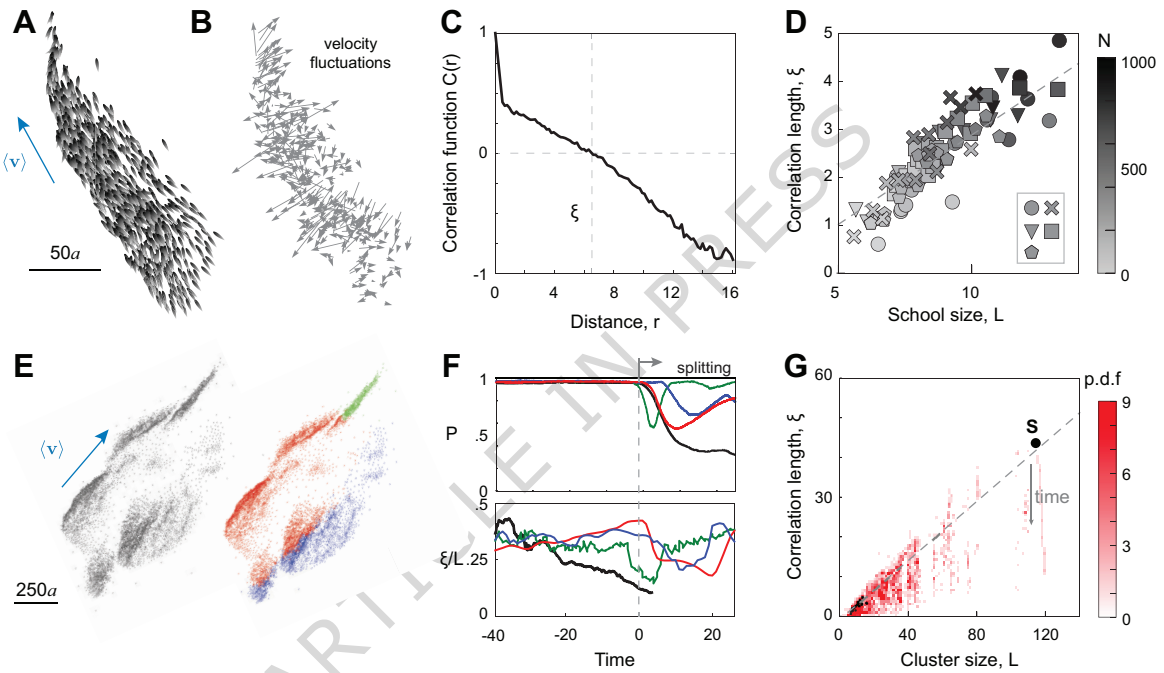

Figure 4: **Scale-free correlations in velocity fluctuations are compromised during school reorganization and fragmentation.** **A.** A snapshot of a stable and cohesive school of $N = 1000$ swimmers and **B.** corresponding velocity fluctuations. **C.** Correlation function $C(r)$ (5) in velocity fluctuations between pairs of swimmers as a function of their mutual distance r. **D.** The correlation length ξ is linear in school size $L = \max\|\mathbf{x}_i - \mathbf{x}_j\|$, with $\xi \approx 0.37L - 0.84$, and coefficient of determination $R^2 = 0.83$, for all alignment and noise intensities in the cohesive and polarized regime; here, (I_a, I_n) are given by $\circ : (9, 0.5)$, $\times : (7, 0.5)$, $\nabla : (5, 0.5)$, $\square : (9, 0.3)$, $\pentagon$: $(9, 0.7)$. The fitting slopes for each parameter set separately are given in Tab .S2. Grey scale indicates the number of fish N. **E.** Snapshots of school with $10,000$ fishes prior to split. The right panel shows the coloring based on the clusters after splitting. **F.** Polar order parameter P and correlation length over school size ξ/L for the whole group (black) and individual clusters (red, blue, and green with corresponding colors). **G.** Histogram of correlation length and cluster size for all clusters emerging in the simulation of $10,000$ fish.

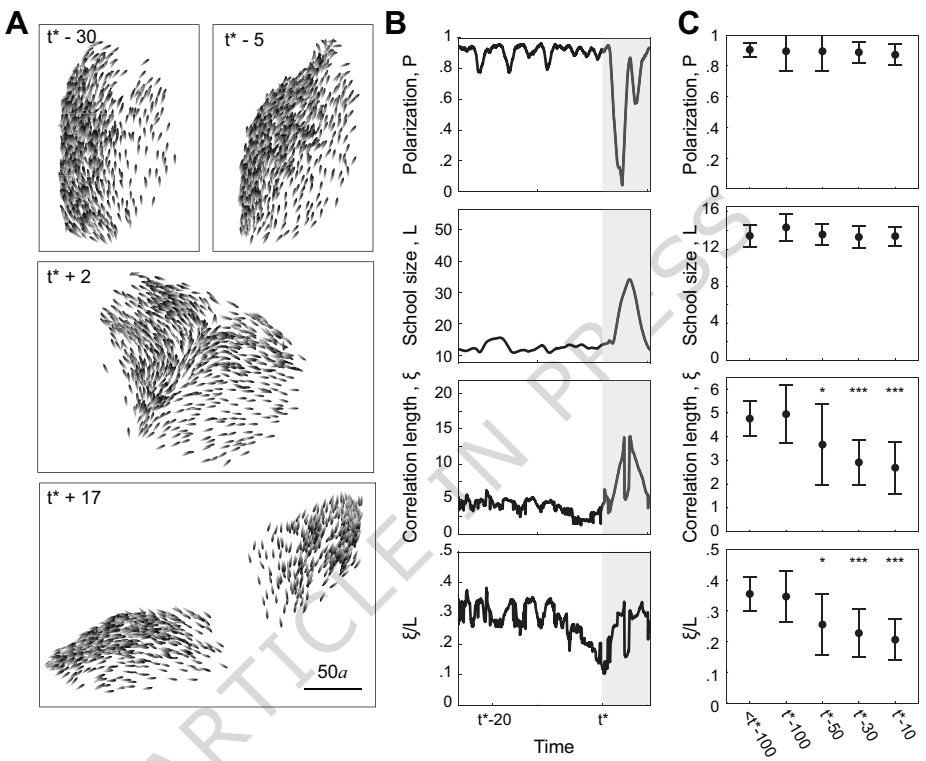

Figure 5: **Loss of scale-free correlations prior to fragmentation. A.** Snapshots of a school with 1000 fish prior to splitting and during splitting and merging. **B.** Time evolution of polar order parameter P, school size L, correlation length ξ, and ratio of correlation length to school size ξ/L spanning a time window before and during a splitting and merging event, the latter highlighted in gray. **C.** P, L, ξ, and ξ/L based on statistics taken from 10 Monte Carlo Simulations of time-average values taken over time windows $t \in [t^{\dagger}, t^* - 100]$, $[t^* - 100, t^*]$, $[t^* - 50, t^*]$, $[t^* - 30, t^*]$, $[t^* - 10, t^*]$, where t^* indicates the onset of a splitting event and $t^{\dagger}$ indicates the end of merging following a prior splitting event. Data points are represented by mean values +/- standard deviations. To evaluate the difference in the statistical properties of these histograms, a two-sample t-test is used [92, 93]. The null hypothesis states that there is no significant difference in the statistics. A smaller p-value indicates stronger evidence against the null hypothesis, suggesting a more significant difference in performance. * $p < 0.05$, ** $p < 0.01$, *** $p < 0.001$. Using the values at $t \in [t^{\dagger}, t^* - 100]$ as baseline, and values from $[t^* - 100, t^*]$, $[t^* - 50, t^*]$, $[t^* - 30, t^*]$, $[t^* - 10, t^*]$ are reported in order, two-sided p-values are: for polarization P: 0.82, 0.82, 0.51, 0.21; for school size L: 0.12, 0.75, 0.77, 0.93; for correlation length ξ: 0.67, 0.096, 1.8×10^{-4}, 3.0×10^{-4}; for ξ/L: 0.78, 0.018, 8.3×10^{-4}, 6.1×10^{-5}.

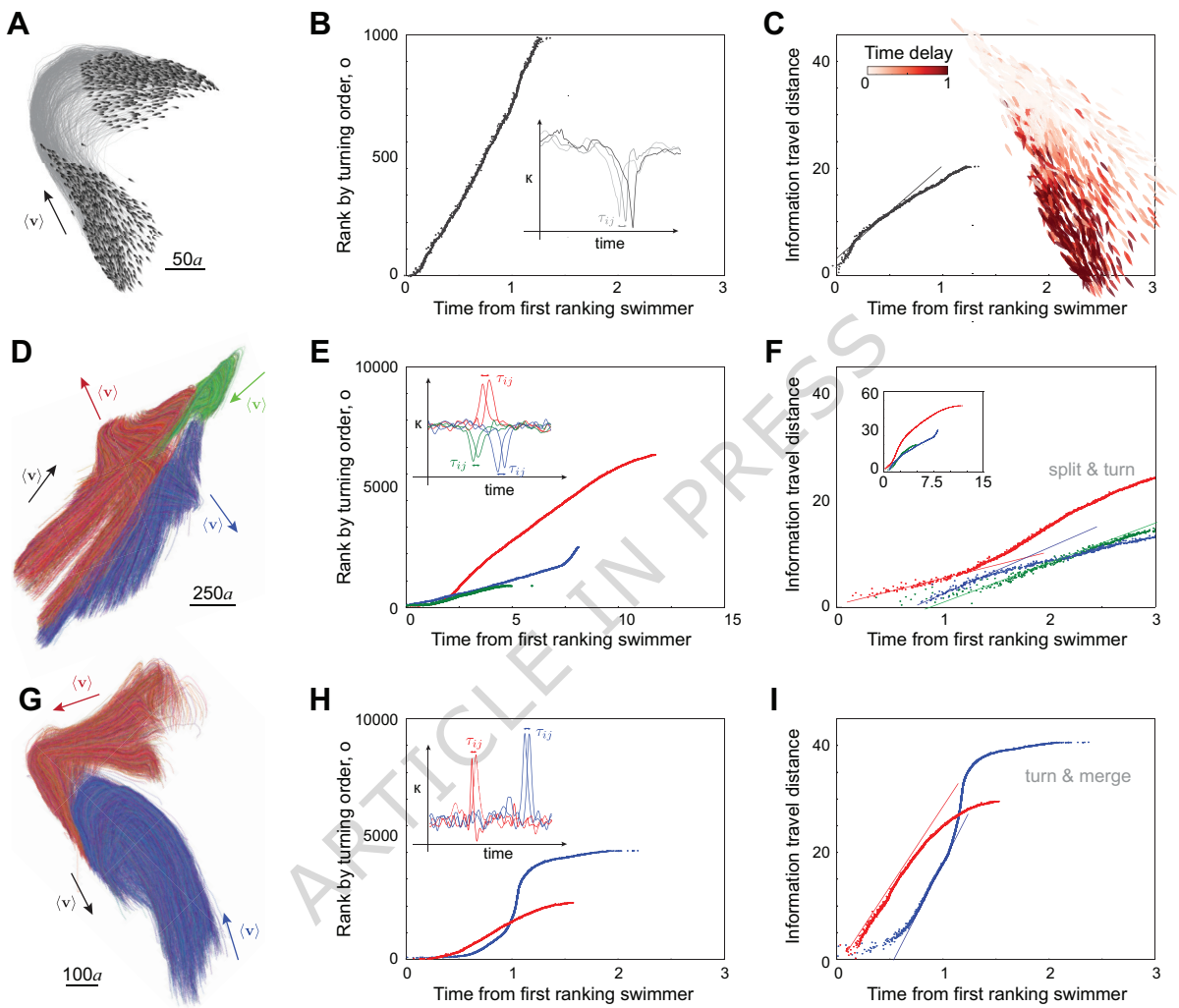

Figure 6: **Information transfer during turning, splitting and merging. A.** Polarized school of $N = 1000$ swimmers turns spontaneously by "free will". **B.** Rank of fish by the order o at which they reach maximal curvature (inset) and **D.** information travel distance defined as $\sqrt{o/\text{density}}$ versus absolute turning time delay; slope indicates that information travels linearly in time at speed equal to 17 times the self-propelled speed U. Inset shows absolute turning time as a colormap over all swimmers. P and ξ/L are reported in Fig. S5B. **D.** Trajectories of individual fish in a polarized school of $N = 10{,}000$ swimmers that later split into three clusters highlighted in red, blue, and green (Fig. 4E,F). **E.** Rank of fish within each cluster by the order o at which they reach maximal curvature (inset) and **F.** information travel distance versus the absolute turning time delay; information travels at slower speeds compared to freely turning. Colormap of time delays, P and ξ/L are reported in Fig. S5. **G.** Trajectories of individual fish showing the merging of two clusters highlighted in red and blue, taken from a simulation of $N = 10{,}000$ fish. **H.** Rank of fish within each cluster by the order o at which they reach maximal curvature (inset) and **I.** information travel distance versus absolute turning time delay; information travels at faster speeds compared to freely turning. Colormap of time delays, P and ξ/L are reported in Fig. S5G. For a slow-motion replay of these events, see Suppl. Movie 3.

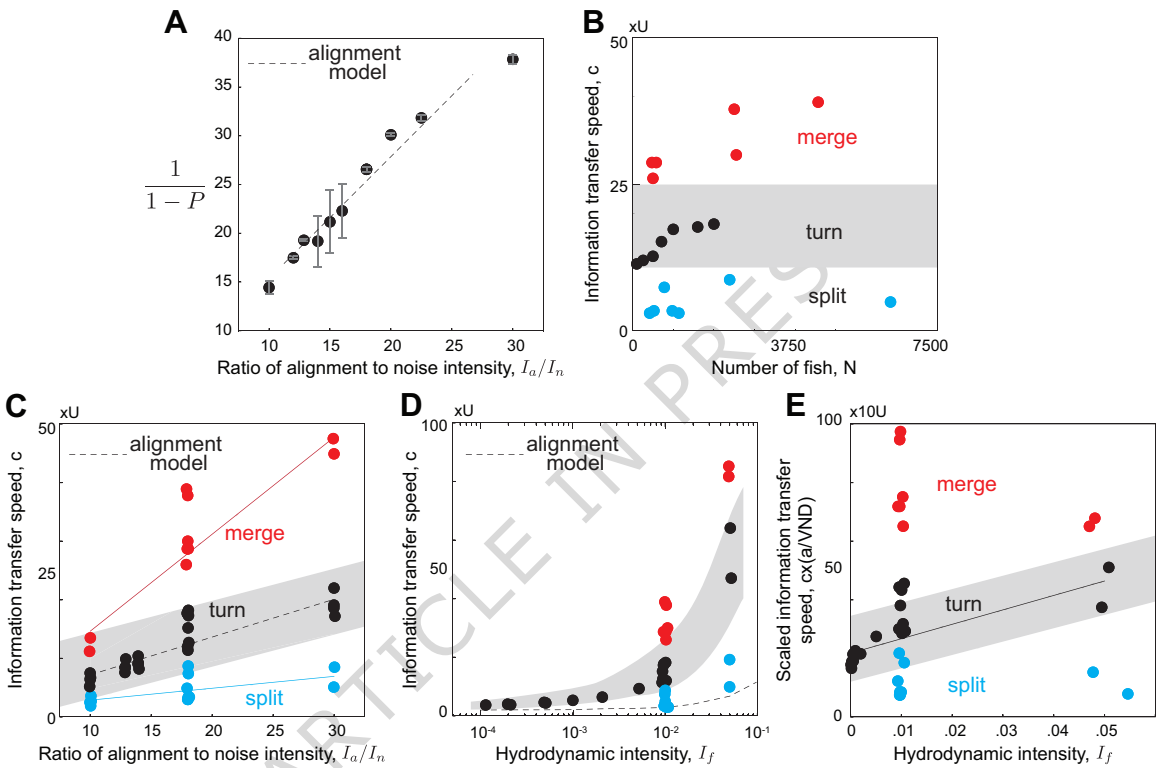

Figure 7: **Flow interactions speed up information transfer. A.** polar order parameter $1/(1-P)$ scales linearly with I_a/I_n fo (see also Fig. S9A,B). The best linear fit is $1/(1-P) = 1.23I_a/I_n + 3.23$ with $R^2 = 0.964$; all results for $N = 100$. Data points represent the average value, and error bar represents standard deviation, number of Monte Carlo simulations is reported in Table S1. **B.** Information travel speed c (in units of U) shows weak dependence on number of swimmers N during turning, splitting, merging for schools with parameters $I_a = 9$, $I_n = 0.5$ and $I_f = 0.01$. **C.** c scales linearly with I_a/I_n; best linear fit gives $c = 0.65I_a/I_n + 0.73$ at $R^2 = 0.92$ during free turning, $c = 0.20I_a/I_n + 0.84$ at $R^2 = 0.98$ during splitting, and $c = 1.65I_a/I_n - 1.91$ at $R^2 = 0.96$ during merging. Results in panels A-C for the same parameter sets (I_a, I_n) in Fig. 4. **D.** c increases with increasing hydrodynamic intensity I_f on logarithmic scale, with the dashed line showing the prediction using the non-reciprocal alignment model $c \sim \alpha I_a$ with $\alpha = \langle \text{VND} \rangle$. **E.** To remove the effects of I_f on $\langle \text{VND} \rangle$ (Fig. S9D), we scaled c with $\langle \text{VND} \rangle / a$. If I_f affects c only through its effect on VND, we expect the scaled speed $c/\langle \text{VND} \rangle$ to be independent of I_f. Instead, it increases linearly with I_f during free turning, with $c/\langle \text{VND} \rangle = 492.46I_f + 21.79$ at $R^2 = 0.77$, indicating that flow interactions increase information travel speed. Results in panels D and E are for $I_a = 9$ and $I_n = 0.5$.

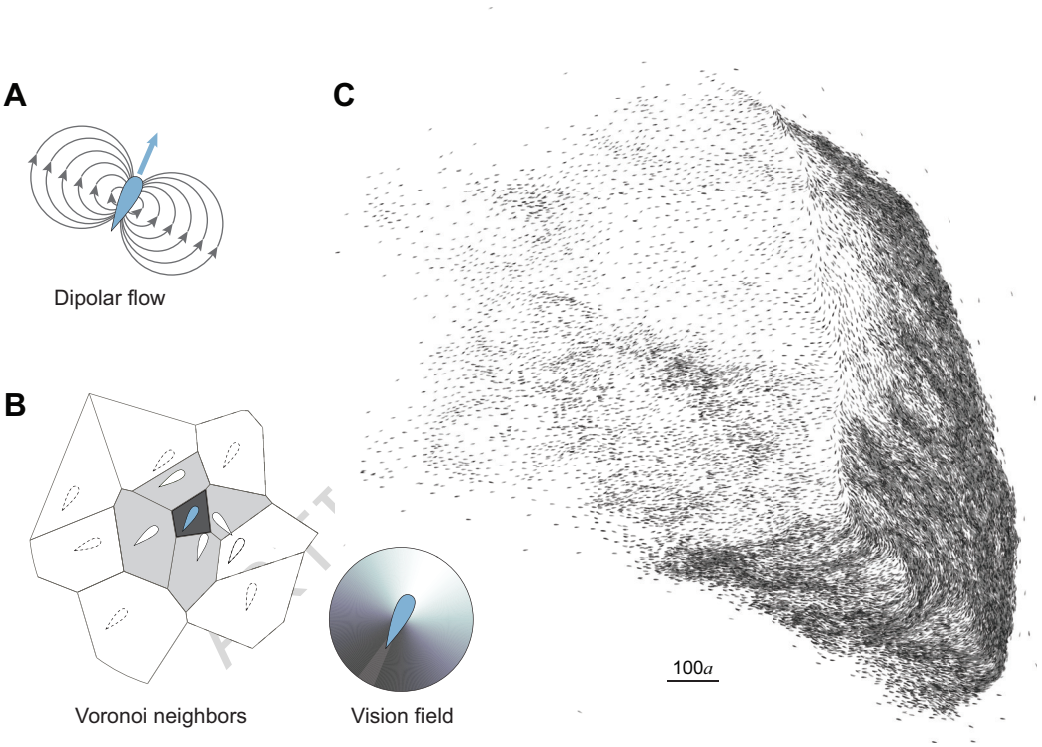
A
Dipolar flow
B
Voronoi neighbors
Vision field
C
100a

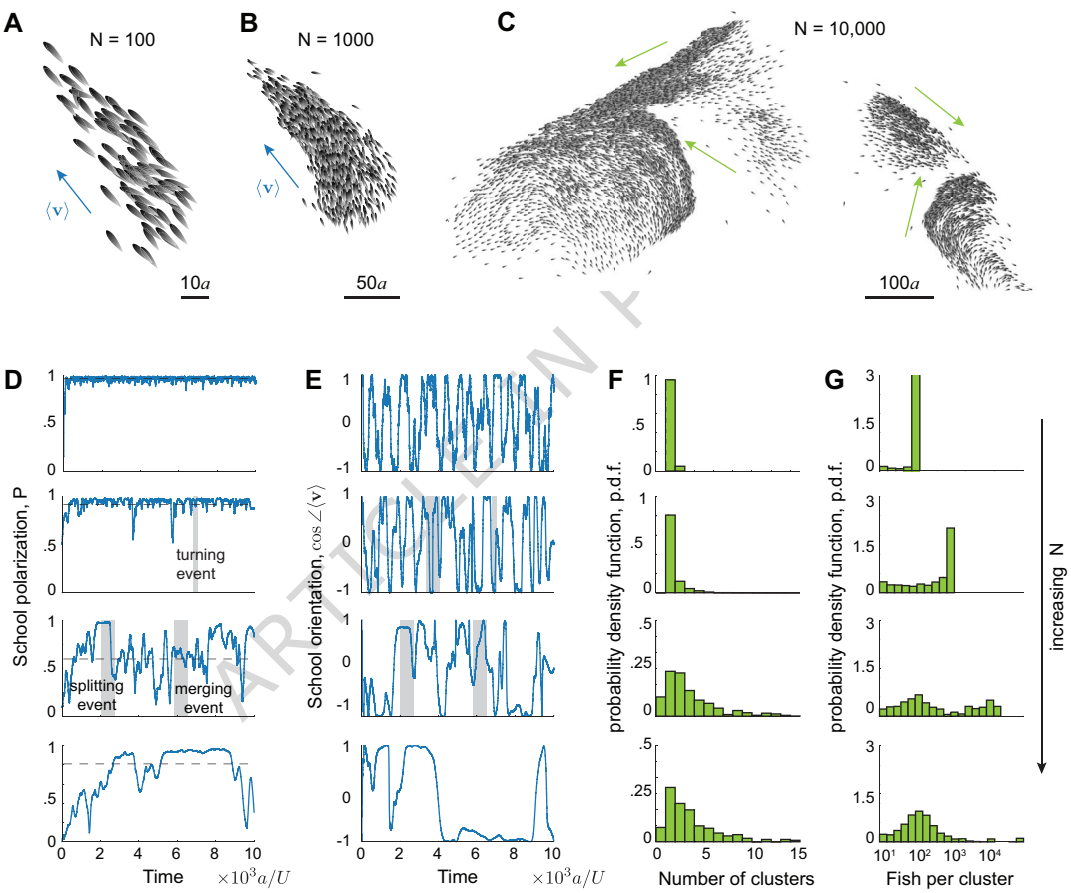
A
N = 100
⟨v⟩
10a
B
N = 1000
⟨v⟩
50a
C
N = 10,000
100a
D
School polarization, P
turning event
splitting event
merging event
Time
×10³a/U
E
School orientation, cos∠⟨v⟩
Time
×10³a/U
F
probability density function, p.d.f.
Number of clusters
G
probability density function, p.d.f.
Fish per cluster
increasing N